ROYAL SOCIETY OF CHEMISTRY

PAPER

Check for updates

Study of the surface reaction kinetics of (La,Sr) MnO₃₋δ oxygen carriers for solar thermochemical fuel production†

YeonJu Kim, [ID] Seung Jin Jeong, [ID] Bonjae Koo, [ID] Siwon Lee, [ID] No Woo Kwak [ID] and WooChul Jung [ID] *

(La,Sr)MnO₃₋δ has received a great deal of attention as an oxygen carrier that can replace the state-of-the-art carrier CeO_2 for solar-driven thermochemical fuel production. Despite the many relevant studies, however, the redox reaction kinetics of this material, which determines the fuel production rate, has rarely been reported. Here, we investigate the surface reaction rate of reduced Sr-doped lanthanum manganite thin films, as a model for a gas/solid interface of a perovskite-structured oxygen carrier under a condition, in which carbon monoxide is produced from CO_2 in a two-step thermochemical cycling process. Thin films of $La_{1-x}Sr_xMnO_{3-\delta}$ (x = 0.1, 0.2, 0.3, 0.4) with dense and flat surfaces are fabricated *via* pulsed laser deposition, and their surface oxygen exchange rates are then characterized *via* electrical conductivity relaxation under actual operating conditions (T = 650 to 800 °C and pO_2 = 2.9×10^{-19} to 9.0×10^{-13} atm). As the Sr content increases, the oxygen exchange greatly decelerates. On the other hand, for a given Sr content, the oxygen exchange does not vary much over a wide range of pO_2 near the target temperature of 800 °C. We also observe the surface oxygen exchange rate has a direct impact on the CO production rate. These observations can guide the selection of an ideal oxygen carrier composition for high-performance fuel production.

Introduction

The need for carbon-neutral, sustainable energy is steadily increasing given the factors of climate change and global population growth. To overcome these challenges, storing solar energy, which is abundant but intermittent, into the form of transportable and dispatchable chemical energy known as solar fuel is emerging as an attractive solution.[1] Among the many technologies which can be used for the synthesis of chemical fuels from sunlight, two-step solar thermochemical fuel production has recently attracted a considerable amount of attention. This technology relies on the capacity of the selected non-stoichiometric metal oxides to release and uptake oxygen in response to changes in the temperature, where solar radiation induces thermal cycling. The resulting stoichiometry changes in the metal oxides can be directly used to produce CO, H_2 or both at the same time when coupled with the introduction of appropriate reactant gases (*e.g.*, CO_2 and H_2O).[2–4] The overall cycle is composed of two steps, as shown in Fig. 1: (1) the thermal reduction of the metal oxides at a high temperature with concentrated solar radiation and the resulting production

of O_2 gas, and (2) the re-oxidation of the partially reduced metal oxides at a lower temperature with an injection of CO_2 and/or H_2O and the subsequent production of CO and/or H_2.

$$(1)\ MO_x \rightarrow MO_{x-\delta} + \frac{\delta}{2}O_2 \tag{1a}$$

$$(2)\ MO_{x-\delta} + \delta H_2O\ (or\ CO_2) \rightarrow MO_x + \delta H_2\ (or\ CO) \tag{1b}$$
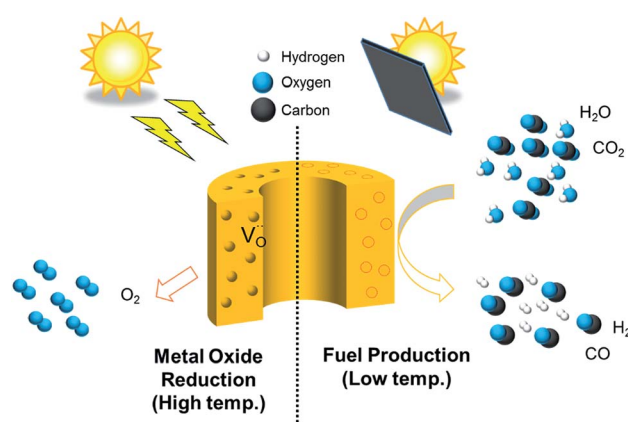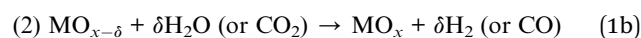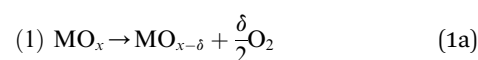

Fig. 1 A schematic image showing the overall solar thermochemical fuel production process.

Department of Materials Science and Engineering, Korea Advanced Institute of Science and Technology (KAIST), Yuseong-gu, Daejeon 34141, Republic of Korea. E-mail: wcjung@kaist.ac.kr

This technology allows the use of the entire solar spectrum and has the advantages of fast kinetics in high-temperature processes, enabling the production of solar fuels at high efficiency and production rates even in the absence of precious-metal catalysts. Furthermore, it has the benefits of straightforward implementation and the inherent temporal separation of the fuel and oxygen gases.[2,5]

To date, fluorite-structured metal oxides are most extensively reported for this purpose, and CeO_2 (ceria) has been at the center of this line of research.[2,6,7] Ceria-based materials have the advantages of high redox capacities, fast reaction kinetics, and decent levels of phase stability. However, they require excessively high temperatures (>1500 °C) for the appropriate amount of oxygen release, which makes heat management and system design difficult and thus hinders the industrial development of this technology. Another class of materials that has recently received much attention as part of the effort to lower the reduction temperature (<1400 °C) is perovskite-structured metal oxides, with materials based on lanthanum manganite ($LaMnO_{3-\delta}$) the most intensively investigated among them.[8–15] Scheffe et al.[8] proposed $La_{1-x}Sr_xMnO_{3-\delta}$ (LSM) as a promising oxygen carrier material for the two-step thermochemical cycling process through a thermodynamic characterizations. A further assessment by Yang et al.[9] revealed that the fuel productivity increases when the Sr composition is $0 \leq x \leq 0.4$, whereas the fuel production rate show the opposite trend. McDaniel et al.[10] demonstrated that the replacement of certain Mn sites with Al is better in terms of the fuel yield, production rate, and durability as compared to CeO_2. Bork et al.[15] demonstrated the competitiveness of the LSM system through calculations of the solar thermochemical efficiency levels with different Sr doping levels using data libraries of the computer coupling of phase diagrams and thermochemistry (CALPHAD). There are also reports of lanthanide-based manganese oxides with different metal ions at the A- and B-sites.[11–14]

Despite these many attempts, most studies have focused on the demonstration of fuel production and the analysis of thermodynamic properties in the LSM system.[8,9,14,15] In contrast, there are few studies of the kinetic properties of LSM as an oxygen carrier, with fewer yet being reported under operating conditions relevant to this technology.[16–19] For the rapid production of fuel gases, the surface oxygen exchange and bulk diffusion of an oxygen ion in oxide carrier materials are important. In addition, surface oxygen exchange is particularly important for LSM oxygen carriers, since thickness of oxygen carrier in the form of porous pellets with microstructures to increase the surface area is much thinner than the critical thickness (L_c) of LSM, which is reported to be in the order of centimeters (0.6 cm for LSM ($x = 0.2$) at 850 °C and pO_2 of 10^{-15} atm).[18] However, to the best of our knowledge, there is only one report of the bulk diffusion and surface reaction kinetics of LSM in relatively reduced atmospheres in which the fuel is produced in a two-step thermochemical cycle.[20] Moreover, the surface reaction rate was studied only for a single composition (20% Sr) in CO/CO_2 atmospheres. Accordingly, the limited results pertaining to the transport properties of LSM make it a great challenge to find an ideal oxygen carrier material for two-step solar thermochemical cycling.

In this regard, we characterized the surface reaction kinetics of LSM thin films over a wide range of compositions under the conditions of CO production in a two-step thermochemical cycle. Films of $La_{1-x}Sr_xMnO_{3-\delta}$ ($x = 0.1, 0.2, 0.3, 0.4$) were fabricated on an $Al_2O_3(0001)$ single-crystal substrate via pulsed laser deposition (PLD). The values of the effective surface oxygen exchange coefficient (k_S) were obtained via electrical conductivity relaxation (ECR) at temperature of 650–800 °C and a pO_2 range of 2.9×10^{-19}–9.0×10^{-13} atm using CO/CO_2 buffer gas mixtures. The morphology and chemical composition of the film surfaces were also investigated using atomic force microscopy (AFM) and X-ray photoelectron spectroscopy (XPS), respectively. The use of thin-film samples with flat and dense surfaces improves the accuracy and reliability of the surface analysis. We observed that the k_S values varied greatly depending on the bulk composition of Sr: the smaller the value of Sr, the higher the value of k_S. On the other hand, for a given Sr composition, k_S does not vary much over a wide range of pO_2 between 2.9×10^{-19} and 9.0×10^{-13} atm near the target temperature of 800 °C. Furthermore, we evaluated the total CO production amount and rate of LSM powders in an isothermal condition. As the Sr content increases, CO production increases, whereas the production rate drops sharply, just as in the surface reaction kinetics results. Conclusively, the tradeoff between the amount and rate of fuel production of LSM, which show opposite tendencies according to changes in the Sr composition, allow the suggestion of the oxygen carrier composition and operating conditions to maximize the performance of a thermochemical reactor.

Experimental

Sample preparation

$La_{1-x}Sr_xMnO_{3-\delta}$ ($x = 0.1, 0.2, 0.3, 0.4$) thin films were prepared by pulsed laser deposition (PLD) from oxide targets of the respective composition of materials. The targets were prepared by the EDTA-citrate complexing method. Stoichiometric amounts of $La(NO_3)_3 \cdot 6H_2O$ (Alfa Aesar, 99.99%), $Sr(NO_3)_2$ (Alfa Aesar, 99.97%), $Mn(CH_3COO)_2 \cdot 4H_2O$ (Sigma-Aldrich, ≥99%) were dissolved in distilled water, and EDTA (Junsei, GR grade) and crystallized citric acid (Junsei, GR grade) were combined with the ratio of 1 : 2 : 1 (total metal ions : citric acid : EDTA), and NH_4OH was used to control pH to 6. The mixture was kept at 80 °C until a gel is formed. The gel was then dried and placed in a heating mantle at 450 °C until it was completely burned. Final calcination was done at 1300 °C for 5 hours under air with the heating and cooling rate of 4 °C min^{-1}, and the powder of LSM samples were obtained. Uniaxial pressing at 30 MPa was followed by cold isostatic pressing at 290 MPa. The oxide targets were obtained after sintering at 1500 °C for 8 hours. Polycrystalline thin films with thickness of 1 μm were prepared via PLD on $Al_2O_3(0001)$ single-crystal substrates (MTI Corporation). The PLD system was operated with a KrF excimer laser (Coherent COMPex Pro 205) emitting at 248 nm and energy of 500 mJ per pulse with a repetition rate 20 Hz. During the ablation process, the substrate temperature and oxygen partial

pressure were kept at 700 °C and 10 mTorr, respectively. After the deposition process, samples were annealed in air at 800 °C for an hour for the crystallization.

Physical and chemical characterization

X-ray diffraction (XRD) measurements were taken on powder samples using Rigaku SmartLab with Cu-Kα radiation (λ = 1.5418 Å) at 40 kV and 200 mA with a scan rate of 5° per minute from 20° to 60°. The crystal structure of the LSM thin films were also characterized by Rigaku Ultima IV with Cu-Kα radiation at 40 kV and 40 mA with a scan rate of 4° per minute in the same range of powder XRD. The grain size, morphology, and surface roughness were characterized by an atomic force microscope (AFM, NX10, Park Systems) analysis. The chemical composition of the initial powders and deposited films were measured using an inductively coupled plasma mass spectrometer (ICP-MS, 7700S, Agilent) in the He mode after dissolution in a (HNO$_3$- : HCl = 7 : 3) solution, focusing on the relative proportions between the cations. X-ray photoelectron spectroscopy (XPS, K-alpha, Thermo VG Scientific) of the surface of LSM thin films was performed under ultrahigh vacuum using Al Kα ($h\nu$ = 1486.6 eV) radiation, a 400 μm-diameter beam of monochromatic X-ray source. All XPS spectra were energy calibrated to the C 1s peak with a binding energy of 284.8 eV. The surface composition of LSM and chemical state of Sr were characterized from XPS spectra based on the Shirley background.

Electrical conductivity relaxation measurement

For the measurement of the conductivity of LSM films, two platinum (Pt) electrodes were applied on the LSM films with 200 nm thickness and 2 mm distance by DC magnetron sputtering (with DC power of 100 W, a working pressure of 10 mTorr under a flow rate of 30 sccm Ar, a deposition rate of 60 nm min^{-1}) using a metal shadow mask. A tube furnace with a K-type thermocouple was used for the measurement at temperature range of 650–800 °C at an interval of 50 °C, and various ratios between CO and CO$_2$ gases (pO$_2$ between 2.9 × 10^{-19} and 9.0 × 10^{-13} atm depending on the temperature) with total 150 sccm was made by mass flow controllers (MFC, Fujikin) for CO/CO$_2$ mixtures (CO : CO$_2$ = 0.5 : 99.5, 1.1 : 98.9, 4.8 : 95.2, 12.3 : 87.7) (Fig. S1(a)†). The sample was first kept at equilibrium and the pO$_2$ was abruptly changed with four-way valve at constant temperature. In-plane conductivity, which reflects the oxygen content in the sample, was measured for every 0.5 seconds until the sample adopts to new equilibrium with applying DC current of 700 μA across the length of the specimen and measured the voltage with chronopotentiometry (CP, VSP-300, Biologic). Both the oxidation and reduction direction of the measurement was carried for each conditions in order to justify the assumption of first order surface oxygen exchange reaction and linear dependency of the conductivity on pO$_2$ (Fig. S3†). The normalized conductivity as a function of time was fitted to a solution of the first order surface oxygen exchange reaction equation using the Origin program as follows:[21]

$$\frac{\sigma(t) - \sigma(0)}{\sigma(\infty) - \sigma(0)} = 1 - \exp\left(-\frac{k_S}{a}t\right) \quad (2)$$

where $\sigma(t)$ is the electrical conductivity at time t, k_S is the surface reaction rate constant, and a is the thickness of the sample. All samples used in this study were well fitted, and reactor flush time was as short as a few seconds (Fig. S2†), much shorter than the conductivity relaxation time of each film.

Feasibility test of the fuel production

The CO production test of LSM powders was carried out with a custom-designed isothermal reactor. Experiments were conducted at atmospheric pressure with a fixed-bed flow quartz reactor having an internal diameter of 11 mm. The catalytic bed, which is composed of the mixture of 1 g of powder LSM and 1 g of silica beads between 0.5 g of silica beads, were loaded on quartz wool placed at the middle of the reactor (Fig. S1(b)†). During the measurements, temperature was kept constant at 800 °C with flowing gas mixture of CO and CO$_2$ with Ar as a gas carrier. The samples were first reduced for 30 minutes under gas mixture composed of 16.13 vol% CO and 83.87 vol% CO$_2$ which corresponds to the effective oxygen partial pressure of 1.0 × 10^{-17} atm at the temperature, which corresponds to the oxygen non-stoichiometry value as thermal reduction at 1400 °C takes place. When the reduction is complete with no detection of CO, the reactor was purged by flowing 100 sccm Ar for 10 minutes and CO$_2$ gas was fed into the reactor for the re-oxidation of LSM. The composition of product gases, which have m/z = 44 (the major peak of CO$_2$), m/z = 28 (the major peak of CO, the secondary peak of CO$_2$), and m/z = 40 (the major peak of Ar), were monitored by a quadrupole mass spectrometer (MS, Pfeiffer vacuum, GSD320) every 0.02 seconds. The measurement results were analyzed and compared with theoretical amount of CO production calculated based on the oxygen non-stoichiometry data.[9]

Results and discussion

Structural and chemical characterization

In this study, powder and thin films were prepared for the measurement of CO production rates and surface reaction kinetics, respectively. The geometry of the films for electrical conductivity relaxation was selected for accuracy of the analysis; the surface reaction limited model with controlled surface morphologies was used. Fig. 2 shows the X-ray diffraction patterns of the powder and thin-film samples of LSM. Sr-doped LaMnO$_3$ is known to have two crystal structures, orthorhombic ($Pnma$) and rhombohedral ($R\bar{3}c$), depending on the Sr content and oxygen non-stoichiometry.[22–25] Consistently, we observed that samples with Sr up to 30% have a orthorhombic structure, whereas 40% Sr exhibits an rhombohedral structure. On the other hand, peaks of thin films are difficult to identify owing to the overshadowing effect caused by intense diffraction signals of the substrate and the peak broadening effect of nano-sized grains. However, it should be noted that strain-free polycrystalline films were prepared because various XRD peaks were observed in 1 μm thick films, too thick to be affected by the
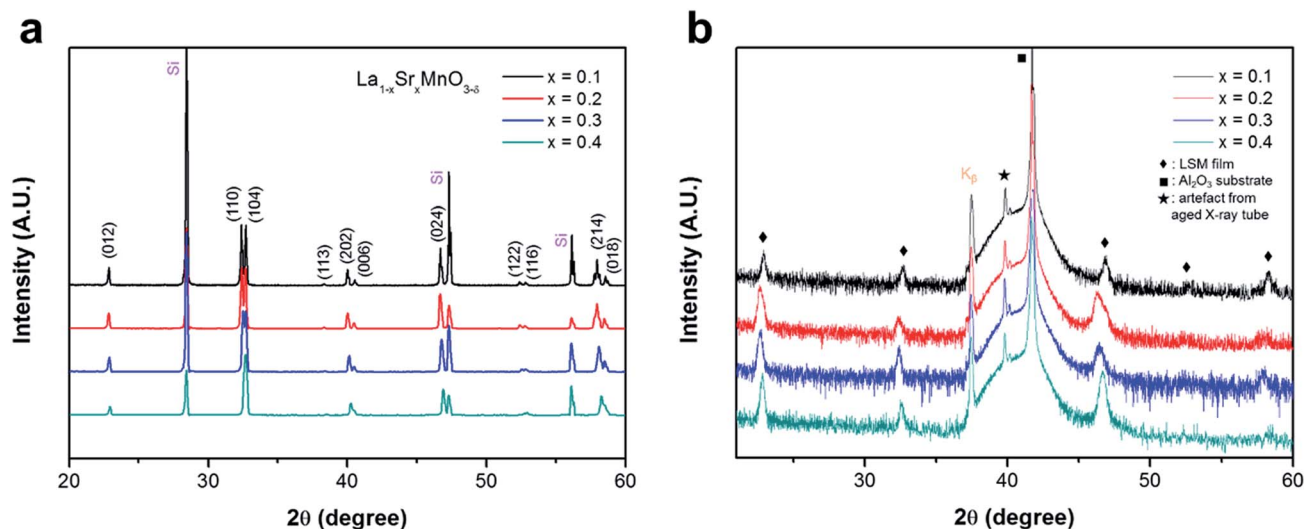
13084 | J. Mater. Chem. A, 2018, 6, 13082–13089

This journal is © The Royal Society of Chemistry 2018

Fig. 2 (a) Powder and (b) thin-film X-ray diffraction patterns of La$_{1-x}$Sr$_x$MnO$_{3-\delta}$ (LSM).
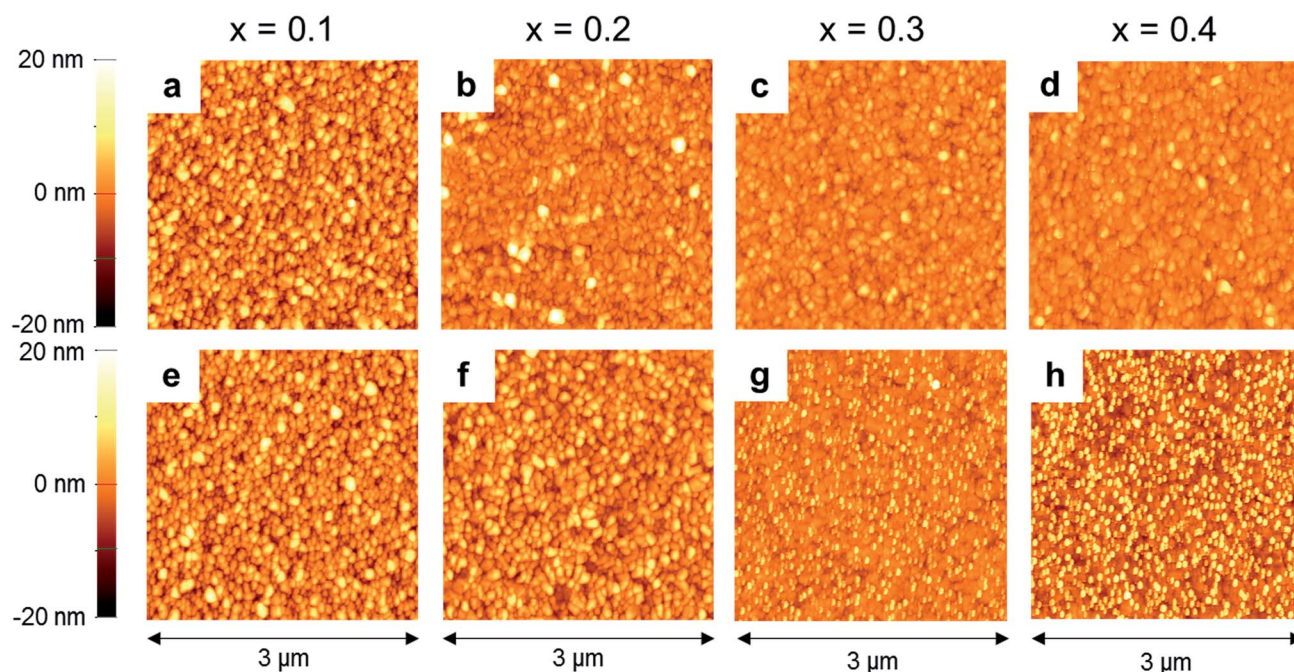

Fig. 3 AFM micrographs of La$_{1-x}$Sr$_x$MnO$_{3-\delta}$ (a–d) before and (e–h) after electrical conductivity relaxation measurements.

lattice strain. In addition, although some reports claim that the orientation of the sample can alter the surface reaction kinetics, we characterized the effect of the Sr concentration, as our LSM thin-film samples have identical orientations without a distinct texture. The chemical compositions of both the powder and thin-film samples analyzed by ICP-MS are also listed in Table S1,† showing that Mn-excess samples with different Sr concentration are synthesized.

One of the essential parameters that can affect the surface reaction rate is the surface morphology. To compare the surface reaction kinetics of LSM thin films with different Sr concentrations quantitatively, the effective surface area and grain size

must be in good agreement for each sample. AFM surface images of 1 μm-thick LSM films are shown in Fig. 3, and the obtained values of the grain size, roughness, and effective surface area using AFM are summarized in Table 1. The film features are consistent with those of typical PLD-synthesized films, such as a flat surface with roughness of less than 5 nm, an actual surface area within 1.022 μm^2 for a 1 μm × 1 μm area, and similar grain sizes for all LSM films with standard deviations of less than 25%. The surface area and grain size of the film are mostly maintained even after electrochemical relaxation measurements at elevated temperatures between 650 °C and 800 °C. Very small particles (about 80 nm), likely Sr

Table 1 Grain size, surface roughness, and surface area of $La_{1-x}Sr_x$-$MnO_{3-\delta}$ films before and after electrical conductivity relaxation measurements as characterized by AFM

| Sr content	Grain size (nm)	Surface roughness (nm)		Surface area in 1 $\mu m \times 1 \mu m$ (μm^2)	
		Before	After	Before	After
0.1	112.0 ± 43.0	4.13	4.15	1.022	1.022
0.2	114.1 ± 41.6	3.38	3.67	1.011	1.017
0.3	133.7 ± 71.4	2.21	2.92	1.006	1.021
0.4	137.4 ± 78.6	2.07	4.85	1.006	1.054

segregates, however, were observed on the surface of the sample containing 30% Sr or more after the heat treatment during ECR measurements (Fig. 3(e–h)). A detailed surface chemical analysis including these particles will be discussed later.

Effect of the Sr concentration on the surface reaction kinetics of LSM

Fig. 4(a) presents the electrical conductivity relaxation profiles of LSM films, showing the transient behavior of the conductivity with a step change in the pO_2 value of the surrounding gas. Here, the conductivity values were normalized by the initial values. A sudden change in pO_2 releases oxygen from the oxide lattice or injects oxygen gas into the lattice until the sample reaches a new thermodynamic equilibrium state. This process consists of two steps: the bulk diffusion of oxygen ions followed by a surface oxygen exchange reaction or *vice versa*. The use of LSM thin films with a thickness of 1 μm, much thinner than the critical thickness (L_c) known to be on the order of centimeters as mentioned above, makes the effect of bulk diffusion negligible.[18] Accordingly, the observed relaxation profiles reflect the reaction rate at the LSM surfaces. The profiles were fit to eqn (2), a representation of the relaxation profile for a first-order reaction at the gas–solid interface, where k_S is the effective surface oxygen exchange coefficient. In addition, the k_S values were in good agreement with previously reported values in reducing environments, as shown in Fig. S4.†

It was found that the oxygen exchange at the LSM surface varies greatly with the Sr content. As is apparent shown in Fig. 3(a and b), the higher the bulk Sr content is, the slower the oxygen exchange become. For example, the k_S value of LSM ($x = 0.1$), obtained at 800 °C with a pO_2 value of 9.0×10^{-15} atm, is more than one order of magnitude greater than that when $x = 0.4$. The faster the surface reaction, the more rapidly the fuel can be produced. Therefore, in terms of the fuel production rate, a low concentration of Sr is advantageous as an oxygen carrier. Conversely, the more Sr there is, the greater the redox capacity of the LSM, and therefore the greater the amount of fuel that can be produced thermodynamically.[9] Therefore, the trade-off between the reaction rate and the redox capacity according to the LSM composition should be properly considered during the material selection process. Details related to this aspect will be discussed later.

At this stage, it is difficult to explain how the oxygen exchange rate of the LSM surface varies with the Sr content.
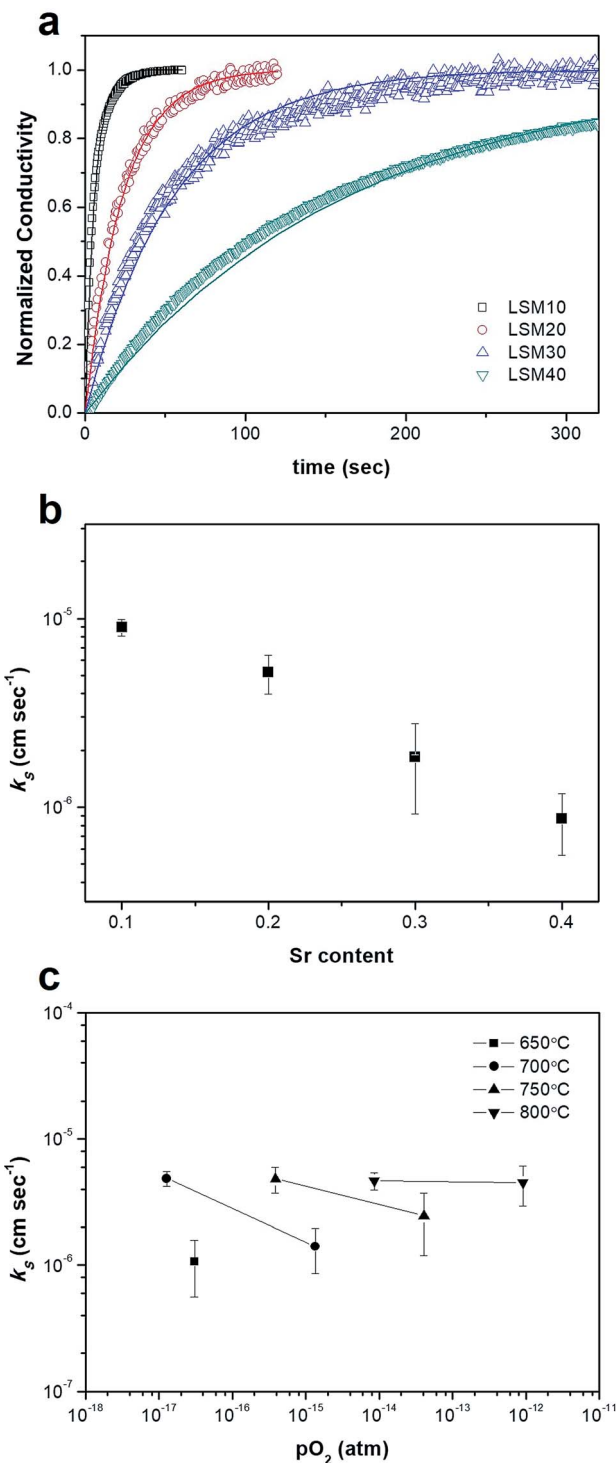
Fig. 4 (a) Relaxation profiles of $La_{1-x}Sr_xMnO_{3-\delta}$ (LSM) thin films with different Sr compositions at 800 °C, $pO_2 = 9.0 \times 10^{-15}$ atm ($\Delta pO_2 = 2.9 \times 10^{-15}$ atm to 1.5×10^{-14} atm), (b) comparison of the k_S values under the same conditions, and (c) surface oxygen exchange coefficients of LSM ($x = 0.2$) for various temperature and pO_2 values under a CO/CO_2 environment. The solid lines in (a) are the fit profiles.

However, we propose surface Sr segregation as a hypothesis explaining this observation. Sr surface segregation and the resulting formation of SrO-like precipitates have been widely

13086 | *J. Mater. Chem. A*, 2018, **6**, 13082–13089

This journal is © The Royal Society of Chemistry 2018

reported to inhibit the surface reactivity of perovskite oxides, including LSM, at high elevated temperatures.[26–30] Given that SrO is an insulator, SrO island precipitates interfere with the oxygen exchange process by passivating the pristine (and thus more reactive) surface of perovskite oxides. To confirm this, we analyzed the surface composition of LSM thin films by XPS. Fig. S5† shows the Sr 3d spectra of a reduced LSM ($x = 0.2$) thin film that consists of two sets of spin–orbit doublets with an energy separation distance of ~1.8 eV and an area ratio of 1.5. The XPS spectra of the same sample obtained after chemically etching the surface for comparison are also shown. The main Sr 3d doublet corresponds to Sr in the bulk lattice, whereas the other doublet with higher binding energy originates from surface Sr species.[27,31] Because the higher energy doublet remarkably disappears after etching, it is apparent that the film surface has a large amount of Sr-excess that is expected to undergo segregation. Table S2† also displays the results of the quantitative analysis by XPS; the surface Sr content of all samples is larger than the bulk, and the surface Sr content increases sharply with an increase in the bulk Sr. Therefore, as the bulk Sr content increases, the degree of Sr segregation on the LSM surface also increases, which may slow the oxygen exchange kinetics. However, given the limited number of experimental results obtained in this study, it is not possible to make a firm conclusion, and further investigations are thus required.

Effects of the temperature and pO_2 on the surface kinetics of LSM

The k_S values over a wide range of temperatures (650 to 800 °C) and pO_2 levels (2.9×10^{-19} to 9.0×10^{-13} atm) with CO/CO_2 are plotted in Fig. 4(c) for LSM ($x = 0.2$). While not enough data

were measured, two aspects are important to note here. First, the isothermal slope of k_S with respect to pO_2 decreases with an increase in the temperature and becomes nearly flat at 800 °C. Because the target temperature for CO production discussed in this study is around 800 °C, we found that the k_S value of LSM is nearly independent of pO_2. This observation is important because the k_S value measured in this study can represent the actual fuel production process of the device that occurs dynamically over a broad range of effective values of pO_2. Second, even LSM ($x = 0.1$), which shows the fastest kinetic characteristics among the four compositions tested, has a smaller k_S value than those of CeO_2-based materials (i.e., 9.0×10^{-5} cm s^{-1} and 6.6×10^{-4} cm s^{-1} at 800 °C, 9.0×10^{-15} atm and 2.3×10^{-15} atm for LSM ($x = 0.1$) and the CeO_2-based material, respectively).[21] Therefore, it is necessary to improve the surface reactivity of LSM further in order to develop an oxygen carrier that far exceeds the state-of-the-art ceria. Various catalytic treatments will be required for this purpose.

CO production rate vs. Sr concentration

To determine the fuel production rate of LSM vs. the Sr content, we examined the CO production half cycle using LSM powders. Here, the LSM powders were lightly reduced at 800 °C and effective pO_2 value was set to 1.0×10^{-17} atm such that they had an oxygen non-stoichiometry value identical to when they underwent a heat treatment at 1400 °C in an inert gas atmosphere.[32] Subsequently, CO_2 was flowed to react with the partially reduced LSM in a packed-bed reactor and the exhaust gas was monitored by a mass spectrometer (MS) after brief purging with an inert gas. The CO production rate was obtained by analyzing the composition of the resultant gas at the given flow
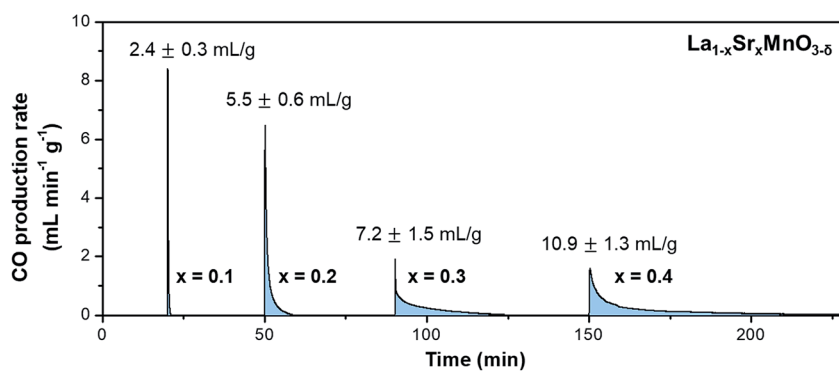

Fig. 5 Effect of Sr composition in $La_{1-x}Sr_xMnO_{3-\delta}$ on thermochemical CO_2 dissociation examined by isothermal reactions.

Table 2 Cycle-averaged CO productivity, production rate, and measurement time of $La_{1-x}Sr_xMnO_{3-\delta}$ powders. All values are based on the profile characteristics and a presumed sufficiently long equilibration time, as well as the estimated time to reach the projected value

Sr content	CO production (mL g^{-1})	Max. production rate (mL g^{-1} min^{-1})	Avg. production rate (mL g^{-1} min^{-1})	Cycle time (min per cycle)
0.1	2.39	8.40	2.03	1.18
0.2	5.52	6.48	1.03	5.34
0.3	7.17	1.93	0.21	34.60
0.4	10.86	1.60	0.14	80.22

This journal is © The Royal Society of Chemistry 2018

J. Mater. Chem. A, 2018, **6**, 13082–13089 | **13087**

rate, and Fig. 5(a) exhibits the typical CO production profiles. As the Sr concentration increases, more time is needed for the completion of the fuel production reactions, at least a minute for LSM ($x = 0.1$) to nearly an hour for LSM ($x = 0.4$). The fuel production characteristics are listed in Table 2. Here, the average production rate is determined by averaging the rate over the time required to complete the fuel production. It should be noted that every characteristic associated with the rate (e.g., the required time, maximum and average rate) becomes slower when the Sr content is increased, which is consistent with the ECR results. On the other hand, the amount of CO production, calculated by integrating the CO production rate over time until the reaction ends, was increased with an increase in the Sr concentration. We observed that LSM ($x = 0.1$) produced the least amount of CO (2.4 mL g^{-1}) and that the production amount increased to 10.9 mL g^{-1} as the Sr content was increased to 40% (Fig. 5(a)), which is consistent with the oxygen non-stoichiometry data of LSM (Fig. S6†).[33,34] Compared to the theoretical amount of CO production derived from oxygen non-stoichiometry data, yields of 50–80% were calculated; the loss is believed to come from the partial oxidation of oxygen carriers during purging of the reactor with Ar after reduction process. A similar trend has been reported with regard to the production of H_2 from H_2O using the same LSM carriers.[9] In fact, this trade-off between the amount and rate of fuel production determines the composition of an oxygen carrier and the cycle condition of thermochemical reactions to maximize CO production in a given operating temperature window (800–1400 °C).

Conclusion

The surface oxygen exchange kinetic properties of (La,Sr) MnO$_{3-\delta}$ thin films were successfully measured via electrical conductivity relaxation (ECR). An analysis of the conductivity relaxation profiles revealed that the surface reaction rate accelerates with a lower Sr concentration under the relevant condition of thermochemical reactions. The fuel production rate evaluated in an isothermal reactor showed a trend identical to that of the surface reaction kinetics, implying the importance of the surface reactivity during the fuel production process. However, the amount of fuel produced, which is determined by thermodynamics, showed the opposite trend. These results suggest the optimization of the material composition and reaction conditions for higher fuel productivity and provide a guideline for a higher fuel production rate by enhancing the surface reaction kinetics of perovskite oxygen carrier materials.

Conflicts of interest

There are no conflicts to declare.

Acknowledgements

Notes and references

1 M. Romero and A. Steinfeld, Energy Environ. Sci., 2012, 5, 9234–9245.

2 W. C. Chueh, C. Falter, M. Abbott, D. Scipio, P. Furler, S. M. Haile and A. Steinfeld, Science, 2010, 330, 1797–1801.

3 P. Furler, J. R. Scheffe and A. Steinfeld, Energy Environ. Sci., 2012, 5, 6098–6103.

4 W. C. Chueh and S. M. Haile, Philos. Trans. R. Soc., A, 2010, 368, 3269–3294.

5 A. Steinfeld, Sol. Energy, 2005, 78, 603–615.

6 P. Furler, J. R. Scheffe and A. Steinfeld, Energy Environ. Sci., 2012, 5, 6098–6103.

7 W. C. Chueh and S. M. Haile, Philos. Trans. R. Soc., A, 2010, 368, 3269–3294.

8 J. R. Scheffe, D. Weibel and A. Steinfeld, Energy Fuels, 2013, 27, 4250–4257.

9 C. K. Yang, Y. Yamazaki, A. Aydin and S. M. Haile, J. Mater. Chem. A, 2014, 2, 13612–13623.

10 A. H. McDaniel, E. C. Miller, D. Arifin, A. Ambrosini, E. N. Coker, R. O'Hayre, W. C. Chueh and J. Tong, Energy Environ. Sci., 2013, 6, 2424–2428.

11 A. Demont and S. Abanades, RSC Adv., 2014, 4, 54885–54891.

12 S. Dey, B. Naidu, A. Govindaraj and C. Rao, Phys. Chem. Chem. Phys., 2015, 17, 122–125.

13 S. Dey, B. Naidu and C. Rao, Chem.–Eur. J., 2015, 21, 7077–7081.

14 T. Cooper, J. R. Scheffe, M. E. Galvez, R. Jacot, G. Patzke and A. Steinfeld, Energy Technol., 2015, 3, 1130–1142.

15 A. H. Bork, E. Povoden-Karadeniz and J. L. Rupp, Adv. Energy Mater., 2017, 7, 1601086.

16 S. Carter, A. Selcuk, R. Chater, J. Kajda, J. Kilner and B. Steele, Solid State Ionics, 1992, 53, 597–605.

17 R. A. De Souza, J. A. Kilner and J. F. Walker, Mater. Lett., 2000, 43, 43–52.

18 L. Yan, K. R. Balasubramaniam, S. Wang, H. Du and P. A. Salvador, Solid State Ionics, 2011, 194, 9–16.

19 L. Yan and P. A. Salvador, ACS Appl. Mater. Interfaces, 2012, 4, 2541–2550.

20 I. Yasuda and M. Hishinuma, J. Solid State Chem., 1996, 123, 382–390.

21 C. B. Gopal and S. M. Haile, J. Mater. Chem. A, 2014, 2, 2405–2417.

22 Q. Huang, A. Santoro, J. Lynn, R. Erwin, J. Borchers, J. Peng and R. Greene, Phys. Rev. B: Condens. Matter Mater. Phys., 1997, 55, 14987.

23 J. F. Mitchell, D. Argyriou, C. Potter, D. Hinks, J. Jorgensen and S. Bader, Phys. Rev. B: Condens. Matter Mater. Phys., 1996, 54, 6172.

24 O. Chmaissem, B. Dabrowski, S. Kolesnik, J. Mais, J. Jorgensen and S. Short, Phys. Rev. B: Condens. Matter Mater. Phys., 2003, 67, 094431.

25 B. Dabrowski, X. Xiong, Z. Bukowski, R. Dybzinski, P. Klamut, J. Siewenie, O. Chmaissem, J. Shaffer, C. Kimball and J. Jorgensen, Phys. Rev. B: Condens. Matter Mater. Phys., 1999, 60, 7006.

26 M. Kubicek, A. Limbeck, T. Frömling, H. Hutter and J. Fleig, *J. Electrochem. Soc.*, 2011, **158**, B727–B734.

27 E. J. Crumlin, E. Mutoro, Z. Liu, M. E. Grass, M. D. Biegalski, Y.-L. Lee, D. Morgan, H. M. Christen, H. Bluhm and Y. Shao-Horn, *Energy Environ. Sci.*, 2012, **5**, 6081–6088.

28 W. Lee, J. W. Han, Y. Chen, Z. Cai and B. Yildiz, *J. Am. Chem. Soc.*, 2013, **135**, 7909–7925.

29 J. Druce, T. Ishihara and J. Kilner, *Solid State Ionics*, 2014, **262**, 893–896.

30 N. Tsvetkov, Q. Lu, L. Sun, E. J. Crumlin and B. Yildiz, *Nat. Mater.*, 2016, **15**, 1010–1016.

31 Z. Cai, M. Kubicek, J. r. Fleig and B. Yildiz, *Chem. Mater.*, 2012, **24**, 1116–1127.

32 A. H. McDaniel, *Solar Thermochemical Water Splitting: Advances in Materials and Methods*, Sandia National Laboratories (SNL-CA), Livermore, CA (United States), 2013.

33 J. Mizusaki, Y. Yonemura, H. Kamata, K. Ohyama, N. Mori, H. Takai, H. Tagawa, M. Dokiya, K. Naraya and T. Sasamoto, *Solid State Ionics*, 2000, **132**, 167–180.

34 J. Mizusaki, N. Mori, H. Takai, Y. Yonemura, H. Minamiue, H. Tagawa, M. Dokiya, H. Inaba, K. Naraya and T. Sasamoto, *Solid State Ionics*, 2000, **129**, 163–177.